

Morphology, rheology and dynamic mechanical properties of PP/EVA/clay nanocomposites

Vahabodin Goodarzi · Seyed Hassan Jafari ·
Hossein Ali Khonakdar · Javad Seyfi

Received: 12 September 2010 / Accepted: 25 February 2011 / Published online: 18 March 2011
© Springer Science+Business Media B.V. 2011

Abstract This paper reports on morphology, rheology and dynamic mechanical properties of polypropylene (PP)/ethylene vinyl acetate (EVA) copolymer/clay nanocomposite system prepared via a single step melt compounding process using a twin screw micro-compounder. Scanning electron microscopic (SEM) investigations revealed that the dispersed phase droplet size was reduced with incorporation of an organo-modified montmorillonite (OMMT). This reduction was more significant in presence of a maleated PP (PP-g-MAH) used as compatibilizer. Phase inversion in the compatibilized blends caused a further decrease in PP droplet size. The OMMT gallery spacing was higher in nanocomposites with EVA as matrix which could be attributed to higher tendency of OMMT nanoparticles towards EVA rather than PP. This enhanced tendency was confirmed by rheological analysis too. Transmission electron microscopy (TEM) results also showed that the majority of OMMT nanoparticles were localized on the interface and within EVA droplets. According to dynamic mechanical analysis, the compatibilized nanocomposites showed higher storage and loss moduli due to better dispersion of OMMT layers. The modulus enhancement of nanocomposites as a function of OMMT volume fraction was modeled by Halpin-Tsai's-Nielsen expression of modulus for nanocomposites. The results of modeling

suggested that the aspect ratio of the intercalated OMMT, in the form of Einstein coefficient (K_E), plays a determining role in the modulus enhancement of nanocomposites.

Keywords Nanocomposites · Morphology · Rheology · Dynamic mechanical properties · Polyolefins · Polypropylene · EVA

Introduction

Material application in industry, medicine and other fields requires precise study on physical and chemical characteristics of the material. Today, scientists as well as industry have found the importance of morphological studies to tailor the product properties and high quality production [1, 2]. The major drawback in polymer blend preparation is immiscibility of the blend components which normally leads to development of a multiphase morphological state. Thus, with controlling interfacial tension as a parameter determining the morphology, physical and mechanical properties can be tailored [3]. Polypropylene (PP) and ethylene vinyl acetate (EVA) copolymer are inherently immiscible and morphology of the obtained blend has not a desired stability [4]. PP is one of the most widely used plastics in large volume. However, its notch sensitivity at low temperatures limits its applications to some extent. Blending PP with elastomers such as EVA has been proposed to compensate this deficiency [5]. Chemical structure of PP and EVA chains are completely different and therefore any sign of interaction or partial miscibility is not probable [6]. Blend compatibilizers such as maleated PP (PP-g-MA) and polyethylene (PE)-g-MA can be utilized to compatibilize the blend [6].

V. Goodarzi · S. H. Jafari (✉) · J. Seyfi
School of Chemical Engineering, College of Engineering,
University of Tehran,
P.O. Box 11155–4563, Tehran, Iran
e-mail: shjafari@ut.ac.ir

H. A. Khonakdar
Iran Polymer and Petrochemical Institute,
P.O. Box 14965/115, Tehran, Iran

Many studies have been focused on the effect of organo-modified montmorillonite (OMMT) on polymer blends and the investigation still continues. Gelfer and coworkers [7] showed that presence of OMMT decreases the dispersed phase particle size in polystyrene (PS)/polymethylmethacrylate (PMMA) blends. Voulgaris and Petridis [8] reported that OMMT plays the role of emulsifier in PS/PMMA blends and showed that this phenomenon increases the melt viscosity of the blend. A similar result was obtained for PS/PP blends system as reported by Wang et al. [9]. They observed that dispersed phase particle size decreases with introduction of OMMT to the system. This was attributed to the role of intercalated OMMT acting as tie molecule for block copolymer formation. Khatua et al. [10] studied the effect of OMMT on morphology of polyamide 6 (PA 6)/ethylene (propylene) random copolymer (EPR) blends. Reduction of dispersed phase particle size was explained by exfoliated OMMT nanoparticles impeding the coalescence of dispersed phase droplets. Li and Shimizu [11] studied the change in morphological state of polyphenylene oxide (PPO)/PA 6 blends with incorporation of OMMT nanoparticles. They reported that OMMT layers localized in PA 6 phase increased the viscosity of PA 6 matrix and this was responsible for suppression of the coalescence of the dispersed PPO droplets.

In our previous work [12, 13], crystallization behavior and thermal degradation of PP/EVA/OMMT nanocomposites were thoroughly investigated. It was found that morphology could play a vital role on final properties of these systems. In the present work the morphological behavior of compatibilized and non-compatibilized PP/EVA blends with different blend compositions are explored and the effect of OMMT dispersion state and its localization on phase separation of blend matrix along with its mechanical and rheological characteristics are discussed.

Experimental

Materials

PP (grade Novolen 1100r) was supplied by Targor Co. (BASF). EVA (grade Escorene Ultra UL00218CC3 with VA content of 18 wt%) was obtained from ExxonMobil Chemical. Maleated PP (PP-g-MA) (grade Polybond 3200) as compatibilizer was procured from Chemtura Co. OMMT used was Nanomer I.44 (Nanocor Inc.) modified with ammonium salt dimethyldialkylammonium halide (70% C18, 26% C16 and 4% C14) [14].

Table 1 Compositions of the prepared PP/EVA blends and nanocomposites

Sample code	PP/EVA ratio (wt%/wt%)	PP-g-MA (wt%)	OMMT (wt%)
P75E25	75/25	–	–
P50E50	50/50	–	–
P25E75	25/75	–	–
P75E25C5	75/25	5	–
P50E50C5	50/50	5	–
P50E50C5O5	50/50	5	5
P25E75C5	25/75	5	–
P25E75C5O5	25/75	5	5
P75E25O5	75/25	–	5
P50E50O5	50/50	–	5
P25E75O5	25/75	–	5
P75E25C5O1	75/25	5	1
P75E25C5O5	75/25	5	5
P75E25C5O7	75/25	5	7
P75E25C7O5	75/25	7	5
P25E75C3O5	25/75	3	5
P25E75C5O3	25/75	5	3

Sample preparation

PP/EVA blends and PP/EVA/OMMT nanocomposites were prepared via a one step process in a conical twin screw DACA micro-compounder. Prior to the melt mixing process all the materials in a specified ratio, were dry premixed and then fed into the micro-compounder. PP/EVA (75/25, 50/50 and 25/75 w/w) blend-based nanocomposites containing 0 to 7 wt% OMMT with 0 to 7 wt% maleated PP (PP-g-MA)

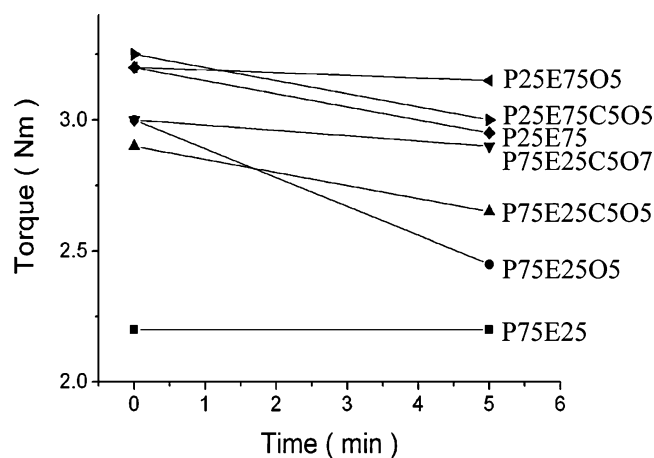


Fig. 1 Variation of microcompounder torque versus temperature during melt compounding of PP/EVA blends and nanocomposites

Fig. 2 Schematic representation of morphological state of blend-based nanocomposites: **a** polymer blend, **b** blend nanocomposite in which nanoparticles are localized in dispersed phase and **c** blend nanocomposite in which nanoparticles are localized in matrix phase



were made. In addition, the neat components (PP and EVA) were melt-mixed separately with 5 wt% OMMT under the similar processing conditions. A processing temperature of 210 °C, a screw speed of 150 rpm, and a mixing time of 5 min were used for preparation of all the blends and nanocomposites. The extruded strands were cooled on an aluminum tray in air. For dynamic mechanical analysis (DMA) the extruded strands were compression molded into rectangular 0.5 mm thick sheets with dimensions of 20 × 10 mm. The molding was performed at 210 °C and a pressure of 10 MPa. The compositions of the prepared samples are presented in Table 1.

Characterization

The wide angle X-ray scattering (WAXS) analysis was done by using an X-ray diffractometer P4 with area detection system GADDS (Siemens AG Karlsruhe, now: BRUKER axs Karlsruhe) operating at 40 kV and 30 mA for Cu K_{α} radiation ($\lambda=0.154$ nm). The samples were investigated in transmission mode with the primary beam

perpendicular to the extrusion direction. The scattering range of 1.8–10° in 2θ was employed. The intensity versus 2θ plots were performed by sectoral integration ($\pm 30^\circ$ in relation to the extrusion direction) with steps $\Delta 2\theta=0.1^\circ$ (mean measuring time $\Delta t=1,200$ s). The dispersion state of the OMMT platelets in the blends was studied by means of a transmission electron microscopy (TEM). Ultra thin sections of the extruded samples (approximately 80 nm thick) were obtained under cryogenic conditions at -120 °C using an EM UC/FC6 ultramicrotome (Leica) equipped with a diamond knife. These ultrathin sections were collected on 300-mesh copper TEM grids and they were investigated by means of a LEO 910 TEM (Carl Zeiss) using an accelerated voltage of 120 kV. The sections were not stained because the EVA-phase would then become too dark for identification of clay nanoparticles in a descriptive way. The chance to distinguish the differences between PP, EVA and the OMMT nanoparticles without staining was good enough. A scanning electron microscopy (SEM) was used to characterize the morphology of the blends and nano-

Fig. 3 SEM images of PP/EVA blends with different blend compositions **a** P75E25, **b** P50E50 and **c** P25E75

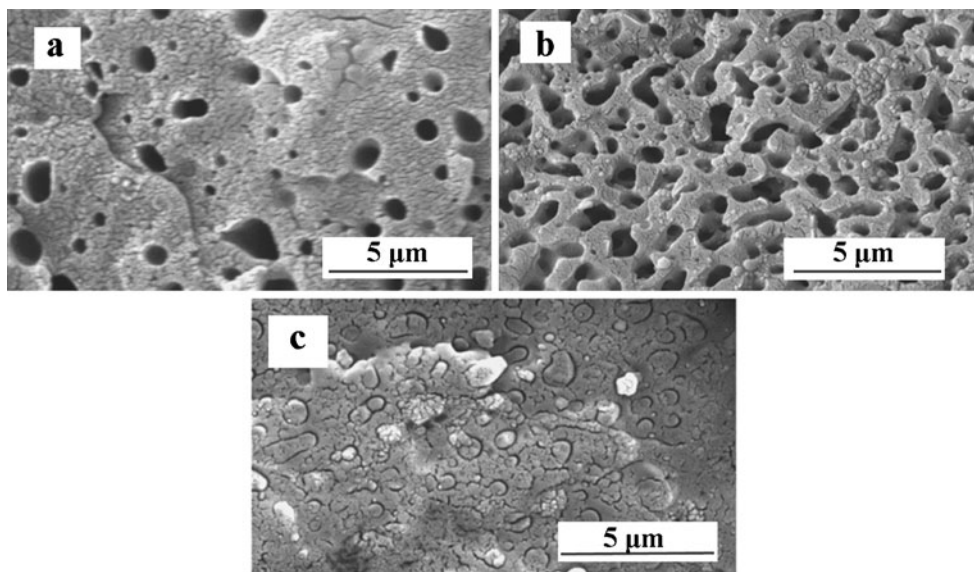
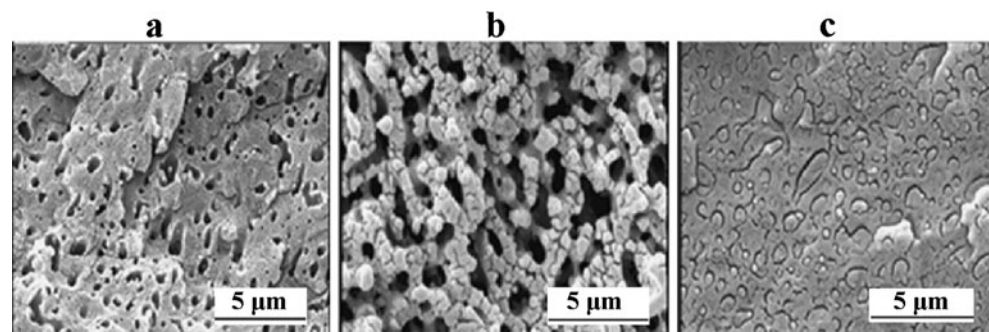


Fig. 4 SEM images depicting effect of PP-g-MA as compatibilizer on PP/EVA blend morphology with different compositions **a** P75E25C5, **b** P50E50C5 and **c** P25E75C5



composites. An extruded strand was immersed in liquid nitrogen for some time and a brittle fracture was performed. The fractured surface was etched in 1, 2-dichloroethane for 1.5 h to remove the EVA phase of the blends and nanocomposites. The etched surfaces after proper drying were gold sputtered and observed under a PHILIPS CM200 SEM. Based on the SEM image analysis, number average particle size (D_n), is calculated by using the following equation:

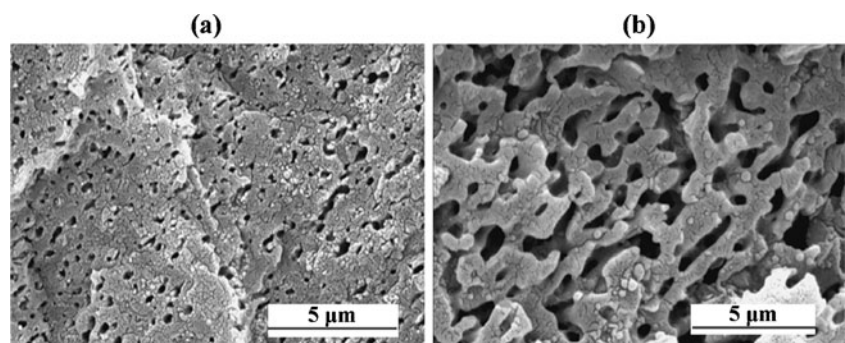
$$D_n = \frac{\sum N_i D_i}{\sum N_i} \quad (1)$$

where N_i is the number of domain droplets in a determined range of diameters, D_i is the diameter of domain droplet, ($\sum N_i = n$) is the total number of domain droplets. Interparticle distance (ζ) in the continuous phase was calculated based on Wu's equation [15]:

$$\zeta = D_n \left\{ (\pi/6\varphi_d)^{1/3} - 1 \right\} \quad (2)$$

where φ_d is the volume fraction of domain phase. Dynamic mechanical analysis (DMA) was performed by means of a DMA2980 (TA Instruments, USA) in a bending mode using a single cantilever clamp at a frequency of 10 Hz, a temperature range of -150 to 150 °C and a heating rate of 3 K/min on the compression molded samples with the dimensions of $20 \times 10 \times 0.5$ mm³.

Fig. 5 Effect of simultaneous incorporation of compatibilizer and OMMT on morphological state of PP/EVA blends **a** P75E25C5O5 and **b** P50E50C5O5



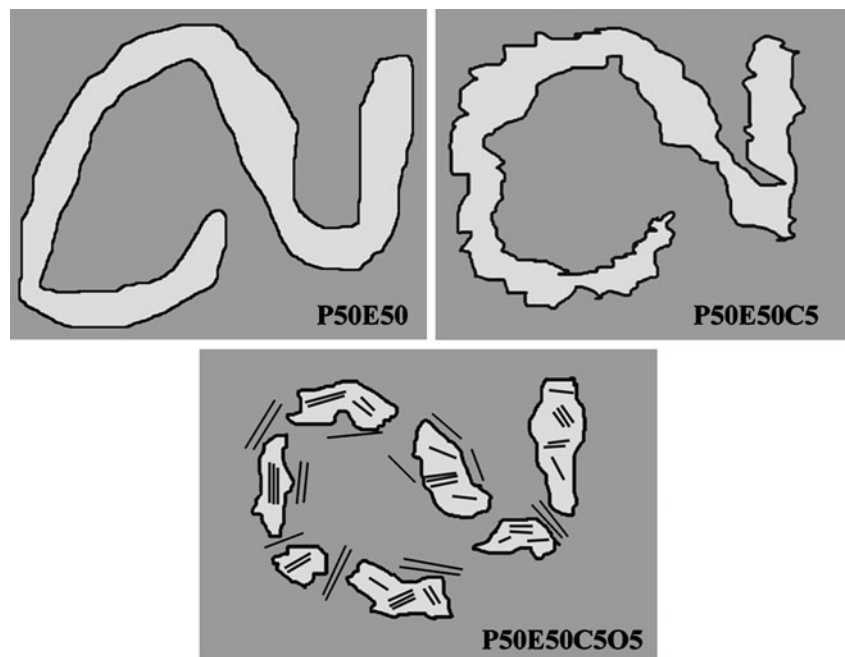
Results and discussions

Morphology of the PP/EVA blends and PP/EVA/OMMT nanocomposites

Surface modification of montmorillonite nanoparticles with organic species decreases its hydrophilicity resulting in a better interaction with hydrophobic polymer matrix. In this state, intercalation/exfoliation of OMMT layers is facilitated thermodynamically. Although, the OMMT used in this study has been already surface treated but its degree of hydrophobicity is not high enough to have a good interaction with PP phase. On the other hand, OMMT particles exhibit a very strong interaction with EVA phase. Thus, it seems that PP/EVA/OMMT system could be an appropriate model to study the effect of OMMT on phase separation of non-compatibilized blend-based nanocomposites.

Figure 1 depicts the change in micro-compounder torque during melt blending for the studied samples as a function of temperature. It is observed that incorporation of OMMT increases the torque in both P75E25 and P25E75 samples. The higher viscosity of nanocomposites as compared to the neat blends can be attributed to the exfoliation/intercalation of OMMT nanoparticles induced by strong interaction between OMMT layers and EVA phase. Figure 2 shows a schematic representation of the morphological state of a non-compatibilized blend-based nanocomposite. According to this figure, OMMT layers are localized either in the matrix or within the dispersed phase droplets.

Fig. 6 Schematic representation of the effect of incorporation of compatibilizer and OMMT on morphology of PP/EVA 50/50 (P50E50) system



The SEM images of PP/EVA blends with different blend compositions are presented in Fig. 3. It is seen that the dispersion of EVA droplets in PP matrix is uniform and the shape of droplets appears to be almost spherical. The average particle size of the EVA droplets for P75E25 sample is about 1.19 μm , while a complete co-continuous morphology is observed for P50E50 sample. For P25E75 sample, a phase inversion occurs and EVA acts as matrix. The average particle size of PP dispersed phase is about 0.75 μm showing a reduction compared to that of the EVA droplets in P75E25 sample. This reduction can be attributed

to the lower viscosity of PP dispersed phase compared to that of EVA matrix providing hydrodynamic forces which dominate capillary forces. This impedes the coalescence of the dispersed phase more significantly and thus results in a finer morphological state.

Effect of PP-g-MA as compatibilizer on PP/EVA blend morphology with different compositions is shown in Fig. 4. One can state that the presence of compatibilizer in the system decreases the interfacial tension between the blend components which results in a significant reduction of the average particle size of dispersed droplets. For P75E25

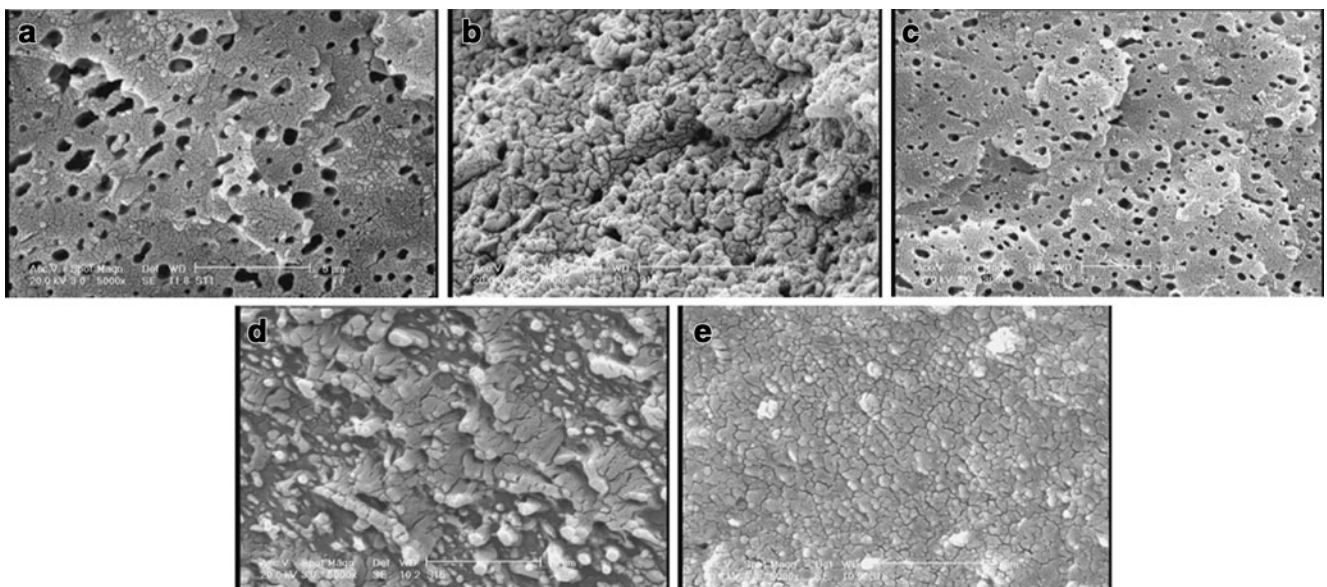


Fig. 7 Effect of variation in content of incorporated blend compatibilizer on morphology of the PP/EVA blend-based nanocomposite **a** P75E25C5O1, **b** P75E25C5O7, **c** P75E25C7O5, **d** P25E75C3O5 and **e** P25E75C5O3. The scale bars are 5 μm

system, addition of 5 wt% compatibilizer decreases the average particle size of EVA phase from 1.19 to 0.68 μm . According to Fig. 4b, inclusion of the compatibilizer results in a coarse co-continuous morphology in P50E50 system. In case of P25E75 blend, the average particle size decreases to 0.54 μm upon addition of 5 wt% of PP-g-MA.

For P75E25 system, incorporation of OMMT decreases the average particle size of the rubber phase to 1.11 from 1.19 μm for the neat blend. It is also observed that addition of OMMT decreases the co-continuity of P50E50 system. For P25E75 system, the average particle size of PP droplets decreases from 0.75 to 0.45 μm upon addition of 5 wt% OMMT. Figure 5 illustrates the effect of simultaneous incorporation of compatibilizer and OMMT on morphological state of PP/EVA blends. This simultaneous incorporation synergistically decreases the average particle size of the dispersed phase as a result of the reduction in interfacial tension. A significant reduction of dispersed phase particle size is detected for P75E25C5O5 and P25E75C5O5 samples as it decreases to 0.32 and 0.22 μm , respectively. Quite interestingly, no trace of co-continuity is observed for P50E50C5O5 which most probably is due to the better interaction between the system counterparts. The effect of addition of OMMT and PP-g-MA into P50E50 system on its final morphology is presented schematically in Fig. 6. Upon addition of compatibilizer into this system, the co-continuity of the blend becomes rougher and then with addition of OMMT, morphology of the system changes to a droplet in matrix type.

The effect of variation in content of incorporated blend compatibilizer on morphology of PP/EVA blend-based nanocomposites is also shown in Fig. 7. It is found that the higher the inclusion of compatibilizer, the finer the obtained morphology. For instance, PP-g-MA inclusion of 1, 3 and 7 wt% in P75E25 system containing 5 wt% OMMT, yields the average particle size of 0.62, 0.32 and 0.28 μm , respectively. (SEM micrographs not shown here) This behavior can be ascribed to the better interaction between the components of system which increases the viscosity and therefore prevents the coalescence of dispersed phase particles. Variation in average particle size of dispersed phase and average distance between particles as a function of OMMT content for blend-based nanocomposites with different blend compositions is shown in Fig. 8a and b, respectively.

Figure 8a shows that as the OMMT inclusion increases, the average particle size of dispersed phase is decreased. Such a decrease is more significant for the compatibilized nanocomposites. It is also noteworthy to mention that in samples with EVA as matrix, a larger reduction in the average particle size of dispersed phase is observed as compared to the samples with PP as matrix. Figure 8b depicts the effect of such inclusion on average distance

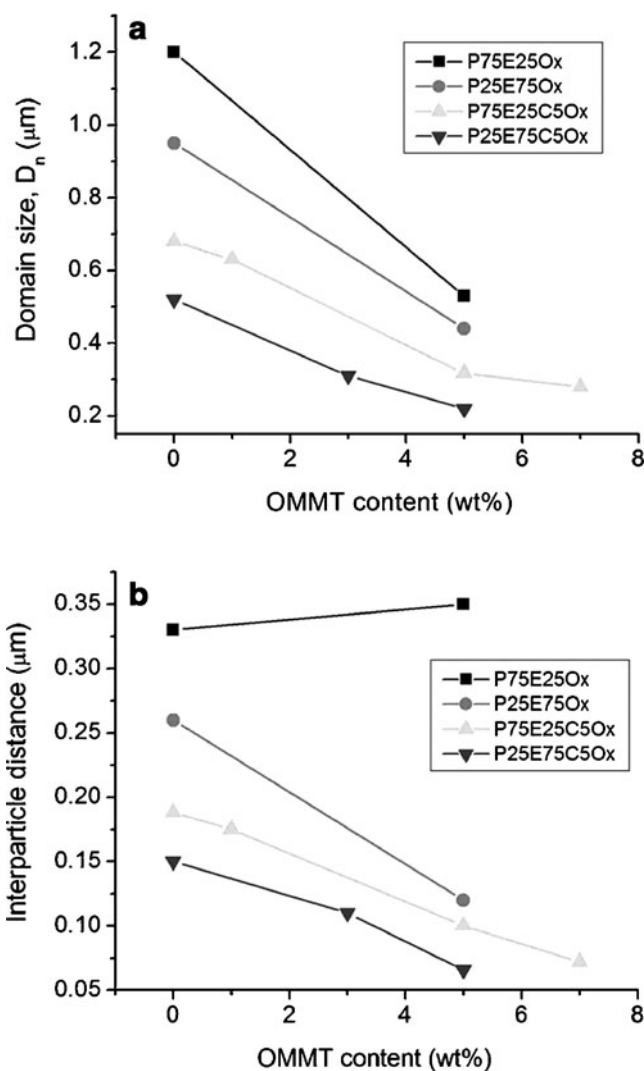
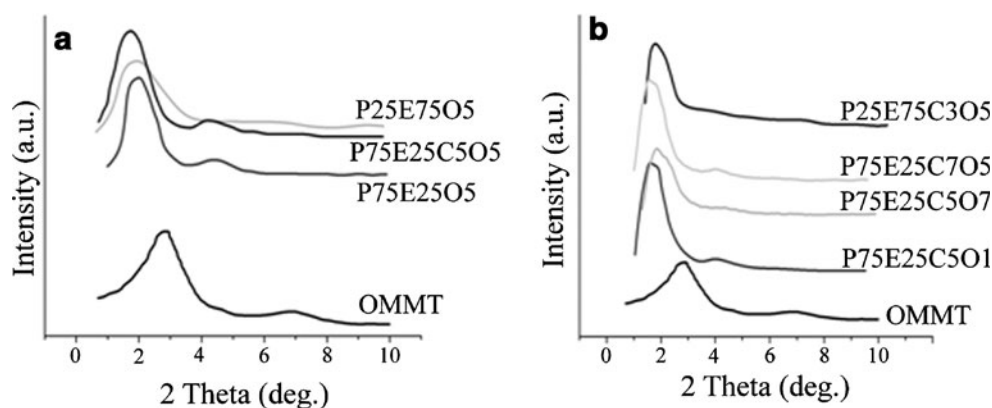


Fig. 8 a Variation in average particle size of dispersed phase and b average distance between particles with change in OMMT inclusion for PP/EVA blend-based nanocomposites with different blend compositions

between dispersed phase particles. It can be concluded that both compatibilizer and OMMT decrease this parameter.

The reduction of dispersed phase particle size with introduction of OMMT into the system could be interpreted using the following theories. First hypothesis is that in initial states of melt intercalation, OMMT nanoparticles may act as sites for concentration of dispersed phase particles. Second postulation is that polymer chains interact with the treated surface of OMMT and play the role of a secondary surface modifier decreasing the interfacial tension. Role of OMMT as a compatibilizer was studied by Khatua et al. [16] in PA 6/linear low density polyethylene (LLDPE). They reported that OMMT layers migrate to the interface of blend counterparts. Localization of both kinds of polymer chains on the surface of OMMT layers creates a graft copolymer which decreases the interfacial

Fig. 9 XRD patterns of neat OMMT and PP/EVA/OMMT nanocomposites with different compositions



tension significantly. Krishnamoorti et al. [17] demonstrated that presence of OMMT affects both enthalpic and dynamic characteristics of nanocomposite systems providing more compatibility between PA 6 and LLDPE as compared to inherent non-compatible counterparts. Third postulation is that OMMT rigid layers increase the viscosity of matrix phase. This could prevent the coalescence of dispersed phase particles which might be due to the reduced mobility of polymer chains in the system. A synergism between all the mentioned postulations is also probable. However, viscosity ratio of PP to EVA can be considered as one of the fundamental parameters determining the morphological characteristics. It seems that great efforts would be necessary to investigate the role of physical/chemical phenomena on the morphology of blend-based nanocomposites.

Structure of nanocomposites

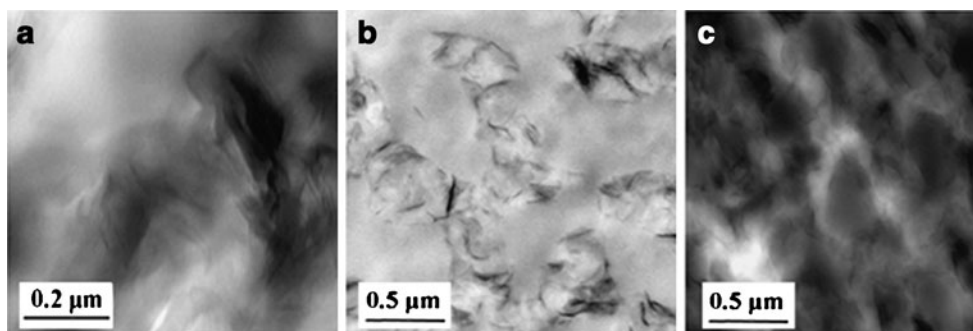
The tendency of nanoparticles to each one of the blend components along with the ability of polymer chain diffusion into gallery interlayer of OMMT is probed by XRD analysis. Figure 9 presents XRD patterns of the neat OMMT and various nanocomposites. The mean interlayer spacing of the (001) plane, $d_{(001)}$, increases from 3.07 nm for the neat OMMT to 3.63 and 4.34 nm for P75E25O5 and P75E25C5O5 samples, respectively which clearly demonstrates the formation of intercalated structure in these systems. Based on these measurements, it is obvious that

incorporation of compatibilizer increases the OMMT interlayer spacing in nanocomposites. The interlayer spacing for the nanocomposites with EVA as matrix is found to be 3.79 nm which is higher than that of the sample with PP as matrix revealing the stronger interaction of EVA chains with OMMT nanoparticles. Moreover, since the width of the basal peak could represent the thickness of silicate layers in nanocomposites, the broader width of diffraction peak for P25E75O5 with respect to that of P75E25O5 could be indicative of more delaminated OMMT layers in this system which again verifies the higher tendency of OMMT nanoparticles towards EVA phase.

Figure 9b shows XRD patterns for the samples with different OMMT inclusion as well as compatibilizer incorporation. During melt intercalation process, the interlayer spacing increases from 3.07 to 4.46 nm with introduction of OMMT to the system. Based on the XRD results, one can conclude that the EVA content in the system is an essential factor to increase interlayer spacing because of its higher polarity as compared to that of PP. It was also observed that with increasing the OMMT inclusion in the system, the interlayer spacing is decreased most probably due to the agglomeration phenomenon. Moreover, a fraction of OMMT species cannot be transformed to individual nanometric layers thus only semi exfoliated/intercalated structure is obtained. It is also possible that some parts remain as non-compatible species in the system [18].

Figure 10 shows TEM images for P75E25C5O5, P50E50C5O5 and P25E75C5O5 samples. These micro-

Fig. 10 TEM images of compatibilized PP/EVA/OMMT nanocomposites **a** P75E25C5O5, **b** P50E50C5O5 and **c** P25E75C5O5



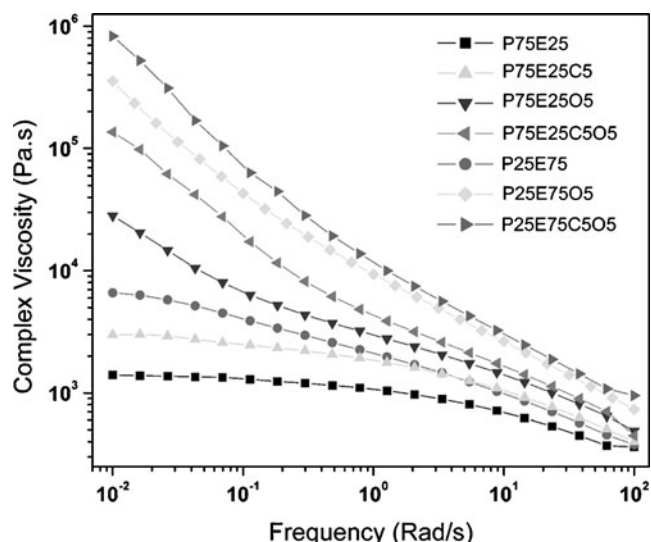


Fig. 11 Complex viscosity versus frequency plots of PP/EVA blends and nanocomposites at 210 °C

graphs clearly exhibit the same behavior presented in Fig. 2. In these images, PP and EVA phases as well as OMMT nanoparticles are easily discernible. According to this figure, it is plainly evident that OMMT nanoparticles tend to localize in EVA phase. This observation is in agreement with the XRD results which revealed the higher interaction of OMMT with EVA rather than PP. TEM images for P75E25C5O5 shows the presence of some thick tactoids in the system. According to the information obtained from TEM and SEM analyses it is proposed that OMMT nanoparticles, localized in EVA phase, can act as a barrier against coalescence and therefore lead to the reduction of the EVA phase particle size.

Rheological behavior

Figure 11 shows complex viscosity, $|\eta^*|$, as a function of frequency for the studied blends and nanocomposites at 210 °C. The first point to notice is the increased viscosity of the blend upon addition of compatibilizer. Several factors could be responsible for this behavior, such as the stiffening of the interface by compatibilizer, enhancement of the dispersion promoted by the presence of compatibilizer, and the total apparent volume of the dispersed phase due to the compatibilizer layer attached to the drop surfaces [19].

It can be seen that addition of 5 wt% OMMT into the non-compatibilized P75E25 system increases the melt viscosity of the system significantly, but the effect of this

OMMT inclusion on pseudo-plasticity of the blend is not as large as expected for polymer-clay nanocomposites. The slope of the viscosity curves increases from -0.04 for P75E25 to -0.56 for P75E25O5. However, simultaneous addition of compatibilizer and OMMT into this blend leads to a further increase in the melt viscosity at low frequencies and also a larger effect on pseudo-plasticity of the system. The reason for this phenomenon could be the higher extent of dispersion of OMMT layers for P75E25C5O5 than that of P75E25O5 which was detected from the higher slope of $\eta^*-\omega$ plot [20].

Based on Table 2, which presents the slopes of $|\eta^*|-\omega$ plots for different samples at the low frequency region, addition of 5 wt% OMMT into the system with EVA as matrix affects its shear thinning behavior more significantly compared to the system with PP as matrix. These results further confirm our previous findings, that is, the high tendency of OMMT to EVA phase due to strong interaction of EVA chains with the clay particles.

Cross-plots, which are very sensitive to the onset of solid-like behavior, are constructed and shown in Fig. 12. The cross-plots for P75E25C5O5, P25E75O5 and P25E75C5O5 show the divergence of $|\eta^*|$ at finite values of complex modulus (G^*) indicating the formation of interconnected networks of silicate layers which are responsible for the observed apparent yield stress. However, the complete yielding phenomenon can be observed just for P25E75C5O5 sample (slope of $|\eta^*|=-1$).

Dynamic mechanical properties

Temperature dependence of the storage modulus (E') and the loss modulus (E'') of various PP/EVA blend and nanocomposites are depicted in Fig. 13. It is seen that EVA having inherently lower modulus with respect to PP decreases the modulus of PP/EVA blends. It is expected that addition of nano-layered silicates into the neat blend causes an increase in storage modulus below the glass transition temperature (T_g). But in case of adding 5 wt% OMMT into the P75E25 system, a reduction in E' is observed which could be ascribed to the lack of strong interactions between the silicate layers and the matrix. Incorporation of both OMMT and compatibilizer in the samples with EVA as matrix increases the modulus more significantly compared to the samples without compatibilizer. It should be noted that, as can be seen in Fig. 13a, at temperatures above the T_g , the reinforcement effect of

Table 2 The slope of $|\eta^*|-\omega$ plots at low frequency region for PP/EVA blends and nanocomposites

Samples	P75E25	P75E25C5	P75E25O5	P75E25C5O5	P25E75	P25E75O5	P25E75C5O5
Slope	-0.04	-0.09	-0.56	-0.85	-0.24	-0.86	-1

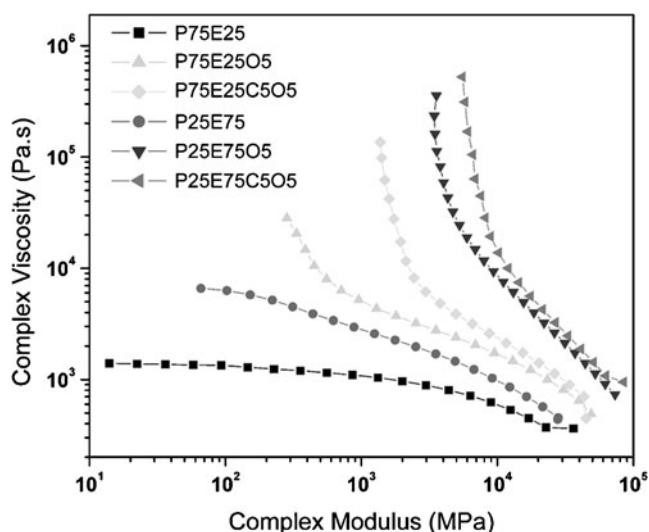


Fig. 12 Cross plots for PP/EVA blends and nanocomposites

OMMT weakens. Krikorian and Pochan [21] suggested that this behavior indicates a weakening of the thermomechanical stability of these materials at high temperatures.

Figure 13b depicts loss modulus of the studied samples. In the samples with PP as the matrix two T_g s can be seen indicating a multiphase morphology for the system. In the samples with EVA as the matrix only one T_g is observed indicating better compatibility and a more refined morphology for this system as compared to the system with PP as matrix.

In order to better compare the effect of adding OMMT to the blend systems on storage modulus, E' values at -70 °C as a function of OMMT concentration for PP/EVA blend-based nanocomposites with different blend compositions are presented in Fig. 14. In case of P75E25Ox samples, the observed decrease in E' values upon addition of 5 wt% OMMT may be due to the weak adhesion between the phases whereas, simultaneous incorporation of OMMT and compatibilizer leads to a monotonous increase in E' values for P75E25C5Ox samples. This behavior could be attributed to the penetration of both polymer and compatibilizer chains into the OMMT layers and their immobilization

Fig. 13 Temperature dependence of (a) storage and (b) loss moduli for PP/EVA blends and nanocomposites

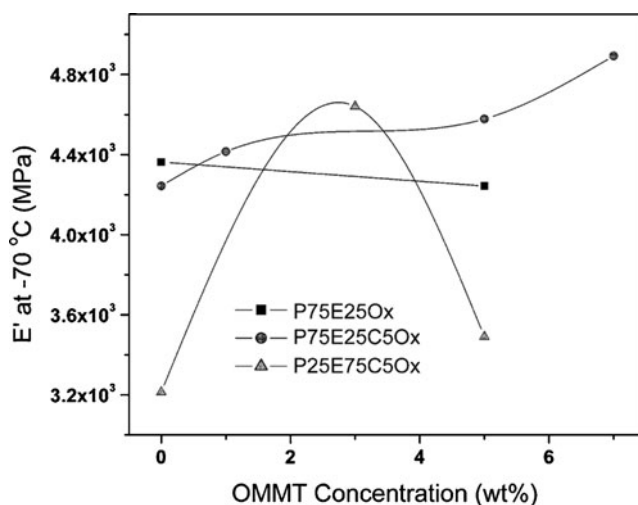
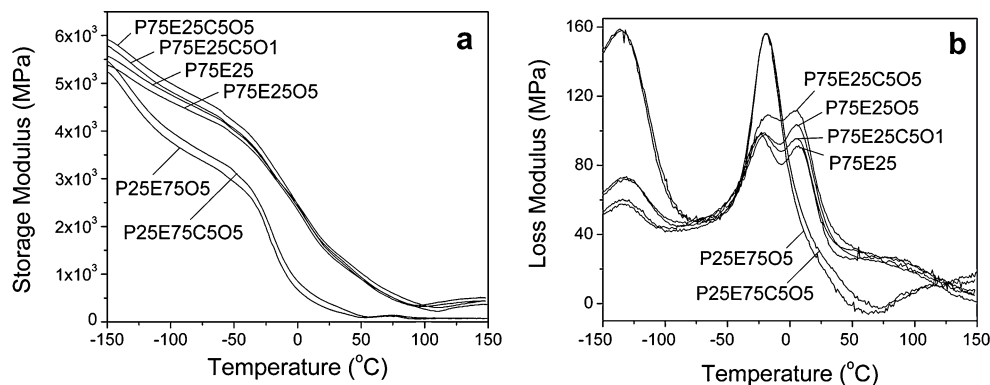


Fig. 14 E' values at -70 °C as a function of OMMT inclusion for different PP/EVA blend-based nanocomposites

inside the silicate galleries. Thus, based on above results, one could conclude that the presence of compatibilizer in P75E25 sample may enhance the dynamic mechanical properties through facilitation of the penetration process of polymer chains into the OMMT layers. A different trend in E' values is seen for P25E75C5Ox samples, that is, a significant increase with addition of 3 wt% OMMT and then a decrease with increasing the OMMT content to 5 wt%. Since nanocomposites with EVA as matrix exhibit a better dispersion of OMMT layers, more penetration of OMMT layers and their immobilization inside the clay galleries in these systems is expected. This could be one of the reasons for significant improvement of storage modulus upon addition of 3 wt% OMMT. However, the monotonous trend observed for the samples with PP as matrix cannot be observed for the samples with EVA as matrix.

It is known that the essential factor governing the enhancement of mechanical properties in the clay-containing nanocomposites is the aspect ratio of the dispersed clay [22]. In order to estimate the aspect ratio of OMMT nanoparticles in the studied samples, the Einstein coefficient (K_E), which represents the aspect ratio (L/D) of

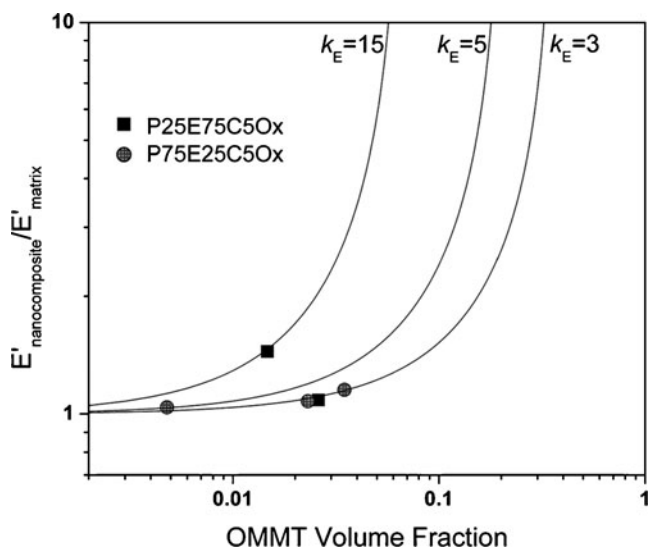


Fig. 15 The composition dependence of $E'_{nanocomposite}/E'_{matrix}$ for PP/EVA/OMMT nanocomposites. The lines show the modeled results by Halpin and Tsai's theory with various K_E

clay particles, is derived by using Halpin and Tsai's theoretical expression modified by Nielsen [23]. Halpin-Tsai's-Nielsen expression of the modulus of nanocomposites is as follows:

$$\frac{E'_{nanocomposite}}{E'_{matrix}} = \frac{1 + XY\phi_{OMMT}}{1 - X\psi\phi_{OMMT}} \tag{3}$$

Where

$$X = k_E - 1 \tag{4}$$

$$Y = \frac{[E'_{OMMT}/E'_{matrix}] - 1}{[E'_{OMMT}/E'_{matrix}] + X} \tag{5}$$

$$\psi = 1 + \left[\frac{1 - \phi_m}{\phi_m^2} \right] \phi_{OMMT} \tag{6}$$

X is a constant related to the aspect ratio, and ϕ_{OMMT} and ϕ_m are the volume fraction of OMMT nanoparticles and the maximum packing volume fraction of OMMT. According to Ray and Okamoto [24] the maximum packing volume fraction of OMMT is equal to 0.63. However, one should note that the value of 0.63 is for spheres with random close packing and platelets of organo-clay either in exfoliated or

in intercalated states, are of disk type. Therefore, using the maximum packing volume fraction of spheres for tactoids or single platelets may lead to some errors in estimation of the aspect ratio of OMMT nanoparticles. Taking the modulus of OMMT to be 170 GPa [25], the composition dependence of $E'_{nanocomposite}/E'_{matrix}$ is calculated according to Eqs. (3), (4), (5) and (6) and the results are presented in Fig. 15. The values of K_E were estimated by selecting an appropriate value for the best fit to the experimentally obtained $E'_{nanocomposite}/E'_{matrix}$ versus OMMT volume fraction plots. K_E is a function of the interaction between the filler and the matrix as well as the aspect ratio of the filler. One could state that the stronger the interaction and the higher the aspect ratio of the filler, the higher the K_E is. The strong interaction between the OMMT and the polymer chains ensures a non-slippage interface. Under the non-slippage condition [26]:

$$K_E = 2.5(L/D)^{0.645} \tag{7}$$

The values of estimated K_E and L/D of OMMT nanoparticles are reported in Table 3. The highest aspect ratio is observed for P25E75C5O3 which, according to Fig. 13a, showed a significant increase in the E' values. By taking a glance at Table 3, the reason for the loss in E' upon increasing of OMMT content to 5 wt% could be found, that is the reduction in the aspect ratio of OMMT nanoparticles. This could be explained by the fact that as the OMMT inclusion increases to 5 wt%, due to the strong edge-edge interaction between the layered silicates, the length of the OMMT particles increases remarkably resulting in a decrease in the overall aspect ratio.

According to Table 3, despite higher aspect ratio of OMMT particles in P75E25C5O5 as compared to P75E25C5O5 and P75E25C5O7, its storage modulus is lower than these two aforementioned samples which is due to the mechanical reinforcement effect of OMMT. It is also worth mentioning that the aspect ratio of OMMT particles increases as the OMMT content increases from 5 to 7 wt%. The reason could be due to the fact that the increase in OMMT loading leads to a higher viscosity of the nanocomposites, and thus, to a higher shear level during the mixing process. It was shown that high shear level improves the delamination of the silicate layers [27]. For nanoclays, the aspect ratios (diameter/thickness) are

Table 3 Estimated Einstein coefficient (K_E) and aspect ratio (L/D) for intercalated OMMT nanoparticles in different PP/EVA/OMMT nanocomposites according to Halpin-Tsai's model

Samples	P75E25C5O1	P75E2C5O5	P75E25C5O7	P25E75C5O3	P25E75C5O5
K_E	5	2.8	3.5	15	3
L/D	3	1.2	1.7	16	1.35

normally very high for individual platelets and tactoids. The values obtained for aspect ratio of clay in different samples seems to be unrealistic due to the model assumptions. However, the obtained values can be compared relative to each other. Based on the data reported in Table 3, the P25E75C5O3 sample has the highest clay aspect ratio and the morphological results confirm this finding.

Conclusions

In this study, a simple model based on polypropylene (PP) and ethylene vinyl acetate copolymer (EVA) was used to investigate the morphology, rheological behavior and dynamic mechanical properties of blend-based nanocomposites. All the blends and blend-based nanocomposites were prepared through a melt intercalation method using a micro-compounder. It was found that both OMMT as nanofiller and PP-g-MA as compatibilizer play a crucial role in reducing the dispersed phase particle size to the submicron level. Among all the mentioned postulations for this phenomenon, viscosity ratio of PP to EVA can be considered as one of the most essential factors governing the final morphology of the system. TEM and XRD results revealed that OMMT nanoparticles tend to localize within the EVA phase. Rheological response further verified this phenomenon and showed that localization of OMMT in EVA phase forms network structures leading to yield stress at low frequency region. DMA results showed that incorporation of OMMT in the absence of compatibilizer led to a reduction in storage modulus of the system while simultaneous incorporation of OMMT and PP-g-MA increased the modulus. Halpin-Tsai's-Nielsen expression of the modulus for nanocomposites was used to estimate the Einstein coefficient (K_E) and consequently the aspect ratio of OMMT nanoparticles. The highest aspect ratio was observed for P25E75C5O3, while further increment of OMMT inclusion caused a reduction in K_E values which was attributed to the strong edge-edge interaction between the layered silicates leading to formation of aggregates in the system. Based on the loss modulus results, nanocomposites with EVA as the matrix exhibited just one T_g , whereas for nanocomposites with PP as matrix, two obvious T_g s were detected. This indicated a

larger compatibility in the systems when EVA is the matrix due to the reduction of dispersed phase average particle size which stemmed from the higher tendency of OMMT to the matrix phase.

Acknowledgment The authors wish to thank the Iranian Nanotechnology Initiative for a partial financial support.

References

- Shonaike GO, Simon GP (1999) Polymer blend and alloys. Marcel Dekker, New York
- Carreau PJ, Degee DC, Chhabra RP (1997) Rheology of polymer systems. Hanser, Munich
- Ma CG, Mai YL, Rong MZ, Ruan WH, Zhang MQ (2007) *Comp Sci Tech* 67:2997
- Maciel A, Del-Real A, Garcia-Garduno MV, Oliva E, Manero O, Castano VM (1996) *Polym Int* 41:227
- Ramirez-Vargas E, Navarro-Rodriguez D, Medellin-Rodriguez FJ, Huerta-Martinez BM, Lin JS (2000) *Polym Eng Sci* 40:2241
- Lee JA, Kontopoulou M, Parent JS (2007) *Macromol Rapid Commun* 28:210
- Gelfer MY, Song HH, Liu L, Hsiao BS, Chu B, Rafailovich M, Si M, Zaitsev V (2003) *J Polym Sci, Part B: Polym Phys* 41:44
- Voulgaris D, Petridis D (2002) *Polymer* 43:2213
- Wang Y, Zhang Q, Fu Q (2003) *Macromol Rapid Commun* 24:231
- Khatua BB, Lee DJ, Kim HY, Kim JK (2004) *Macromolecules* 37:2454
- Li Y, Shimizu H (2004) *Polymer* 45:7381
- Goodarzi V, Jafari SH, Khonakdar HA, Monemian SA, Hässler R, Jehnichen D (2009) *J Polym Sci, Part B: Polym Phys* 47:674
- Goodarzi V, Jafari SH, Khonakdar HA, Monemian SA, Mortazavi M (2010) *Polym Degrad Stab* 95:859
- Gopakumar TG, Lee JA, Kontopoulou M, Parent JS (2004) *Polymer* 43:5483
- Wu S (1988) *Polymer* 26:1855
- Khatua BB, Kim JK (2003) *Proceeding of the 3rd annual meeting of the applied rheology center* 19
- Krishnamoorti R, Vaia RA, Giannelis EP (1996) *Chem Mater* 8:1728
- Ranade A, Dsouza NA, Guade B (2002) *Polymer* 43:3759
- Sailer C, Handge UA (2007) *Macromolecules* 40:2019
- Wagener R, Reisinger TJG (2003) *Polymer* 44:7513
- Krikorian V, Pochan D (2003) *Chem Mater* 15:4317
- Okamoto M, Morita S, Kim YH, Kotaka T, Tateyama H (2001) *Polymer* 42:1201
- Nielsen LE (1969) *Appl Polym Symp* 12:249
- Ray SS, Okamoto M (2003) *Prog Polym Sci* 28:1539
- Somoza AM, Tarazona P (1989) *J Chem Phys* 91:517
- Rao Y, Pochan JM (2007) *Macromolecules* 40:290
- Lee SR, Park HM, Lim H, Kang T, Li X, Cho WJ, Ha CS (2002) *Polymer* 43:2495